Nuclear Instruments and Methods in Physics Research A 762 (2014) 77–84

Contents lists available at ScienceDirect

Nuclear Instruments and Methods in Physics Research A

journal homepage: www.elsevier.com/locate/nima

Study on GASTOF – A 10 ps resolution timing detector

Luc Bonnet, Junhui Liao *, Krzysztof Piotrzkowski **

CP3, IRMP, Université Catholique de Louvain, Chemin du Cyclotron, 2, B-1348 Louvain-la-neuve, Belgium

ARTICLE INFO

Article history:
Received 5 August 2013
Received in revised form
19 May 2014
Accepted 2 June 2014
Available online 10 June 2014

Keywords:
GASTOF
Cherenkov gas detector
10 ps time resolution
MCP-PMTs

ABSTRACT

GASTOF (Gas Time Of Flight) is a type of fast-time detector affiliated to the HPS (High Precision Spectrometer) project which is a forward physics collaborator within CMS. It is a picosecond time resolution Cherenkov gas detector using very fast single anode micro-channel plate photomultiplier (Hamamatsu R3809U-50 or Photek 210) as a photon detector. We firstly measured characteristics of these two types of MCP-PMTs by a fast laser pulse in lab. Then two GASTOF detectors both equipped with a Hamamatsu R3809U-50 tube were studied in a beam test at CERN. According to the analysis of beam test data, the average number of photoelectrons (phe) was 2.0 for both phototubes. By making a cut on the number of photoelectrons such that the mean phe was 3.6 in one phototube and 3.2 in another, we obtained a time resolution of $\sigma \sim 11.7$ picosecond (ps) and $\sigma \sim 8.2$ ps.

1. HPS introduction

The HPS project was started in 2005 as the joint ATLAS+CMS FP420 R&D project, which studied the feasibility of installing and operating spectrometers based on silicon trackers and fast-timing detectors in the LHC tunnel at about ± 420 m from the IP (Interaction Points) of ATLAS and CMS. The HPS is the CMS version of FP420. GASTOF is one type of fast timing detectors being considered by HPS (another type is the QUARTIC detector). By measuring both outgoing protons that have lost less than 2% of their longitudinal momentum, in conjunction with a measurement of the associated centrally produced system using the current CMS detectors, a rich program of studies in QCD, electroweak, Higgs and beyond the Standard Model physics is accessible. A prime process of interest is Central Exclusive Production (CEP), $p+p \rightarrow p+\phi+p$, in which the outgoing protons remain intact and the central system ϕ may be a single particle such as a Higgs boson. In order to detect both outgoing protons in the range of momentum loss appropriate for central systems in the ~ 100 GeV/c^2 mass range during nominal high-luminosity operation, proton tagging detectors must be installed close to the outgoing beam in the high-dispersion region 420 m from the interaction points on each side of the CMS experiments [1]. According to the new proposals, at the stage one, HPS will install tagging detectors only at the positions of CMS's IP ± 240 m; at the stage two, HPS will install detectors at both IP ± 240 m and IP ± 420 m [2].

The HPS fast timing detectors must be capable of operating at the LHC design luminosity of $L = 10^{34}$ cm^{-2} s^{-1} in order to be sensitive to femtobarn-level cross-section in the central exclusive channel [pXp]. At these luminosities overlap backgrounds become significant: [p][X][p], the central system [X] and the other two protons originate from three different interactions; or [pp][X], two protons originate from one interaction, while the [X] from another interaction; or [p][Xp], one proton originates from one interaction, while the central system [X] and [p] from another interaction [1]. HPS time of flight (ToF) detectors at 420 m can be used to obtain a large reduction in overlap backgrounds.

We measure the relative arrival time of the two protons, $\Delta t = t_L - t_R$. Under the assumption that these two protons originate from the same event, the z-position of that event can be calculated as $z_{pp} = \frac{1}{2}\Delta t \cdot c$. The uncertainty on z_{pp} is $\delta z_{pp} = (c/\sqrt{2})\delta t$, where δt is the (r.m.s.) time resolution of the proton measurement. We then require a match between the z_{pp} and the vertex position from the central detector, z_{vertex}. In the case of the overlap backgrounds, the protons do not originate from the same event as the central system [X] and so the vertex reconstructed using the time-of-flight technique will not match the vertex observed in the central detector, which implies that a large rejection factor can be obtained [1]. One of the key parameters determining the rejection factor is the proton tagging detector's time resolution "δt". One GASTOF should provide a time resolution of $\delta t \approx 10$ ps.

* Principal corresponding author. Left Université Catholique de Louvain since January 2013.
** Corresponding author.
E-mail addresses: luc.bonnet@uclouvain.be (L. Bonnet), junhui.private@gmail.com (J. Liao), krzysztof.piotrzkowski@uclouvain.be (K. Piotrzkowski).

http://dx.doi.org/10.1016/j.nima.2014.06.003
0168-9002/

2. GASTOF introduction

GASTOF is Gas Time of Flight, a picosecond time resolution Cherenkov gas detector filled with C_4F_{10}.[1] A sketch of the GASTOF is shown in Fig. 1a. The incident protons produce Cherenkov photons in C_4F_{10} that are reflected and focused to the window center of the MCP-PMT (Microchannel plate-photomultiplier tube) by a UV enhanced concave mirror. The stainless steel wall of the GASTOF is very thin, ~ 0.6 mm. And the thickness of the UV enhanced (MgF_2) mirror is also narrow, ~ 3 mm (along the direction of beam). The filled C_4F_{10} gas[2] is at ~ 1.1 atm and has a refractive index (to 200–600 nm wavelength light) of 1.0014 [3], giving a Cherenkov angle ($\beta = 1$) of about 3° [1]. Fig. 1b shows two real GASTOF detectors used for the beam test at CERN.

Two kinds of MCP-PMTs have been examined using a laser test setup, the Hamamatsu R3809U-50 and the Photek 210. The main parameters of two tubes are shown in Table 1[3] [4,5].

3. MCP-PMT laser test

3.1. The laser test setup

Both the R3809U-50 and the Photek 210 tube were studied by a picosecond laser in a lab of Université Catholique de Louvain. The setup for the laser test is shown in Fig. 2. The PiLas (Picosecond Injection Laser) emits 408 nm light with a time jitter of ~ 2 ps [6]. Attenuated by neutral density filters, the light is injected to a MCP-PMT.[4] The resulting signals are recorded using an oscilloscope.[5]

A typical analog signal measured by a Photek 210 tube with a fast laser pulse is shown in Fig. 3.[6]

3.2. Charge fit for the laser test

To know how many photoelectrons the signal of Fig. 3 represented, it is possible to use the following formula to calculate the number of photoelectrons impinged into the pores of the MCP-PMT [4]

$$N\_phe = \frac{signal\ integral}{50\Omega \times Gain \times 1.6 \times 10^{-19}} \tag{1}$$

where "signal integral" is obtained from integrating an analog signal with a unit of volt $\times$ time, "50Ω" is the oscilloscope's input resistance, "Gain" is the MCP's amplification times,[7] "1.6×10^{-19}" is the charge of an electron. Noticing that the MCP-PMT has a good linearity of charge amplification in the case of a few photoelectrons [4], this "*N_ phe*" can in principle be considered as the photoelectrons which the MCP-PMT measured on its anode. However, the gain of a MCP-PMT may degrade along with usage. While it is not simple for common MCP-PMT users to calibrate the gain of a MCP-PMT accurately. So, we cannot figure out the exact number of the photoelectrons for a signal solely by this kind of calculation as shown in formula (1).

Alternatively, we can measure many analog signals, calculate their *N_phe*, fill in a histogram and perform a fit to the histogram. Obtaining a good fit, we can figure out the exact number of photoelectrons by the *N_phe* and fit results.[8] The photoelectron distribution was assumed to be a Poisson one, while the detectors response for a given photoelectron value was assumed to be a Gaussian function. Our fit function therefore is a Poisson function convoluting with (normalized) Gaussian functions. Details are in the following equations[9]:

$$Sum_0 = e^{-\mu} * [Gauss((x - x_{shift}) \cdot x_{scale},\ 0,\ \sigma_0)] \tag{2}$$

$$Sum_n = \sum_{n=1}^{N} \frac{e^{-\mu}}{n!}\mu^n * [Gauss((x - x_{shift}) \cdot x_{scale}, n, \sqrt{n}\ \sigma_1)] \tag{3}$$

$$Fit\_function = y_{scale} \cdot (Sum_0 + Sum_n) \tag{4}$$

The parameters of Eqs. (2)–(4) are described here.[10]

The charge fit for two kinds of the MCP-PMTs is shown in Fig. 4a and b. The *X*-axes of both figures are the *N_phe* with units of 1 "calculated" photoelectrons.[11] The meanings of fit results like "Y_{scale}", "X_{scale}" and "X_{shift}" are the same as Eqs. (2)–(4). The "$\mu_{poisson}$" is the average number of the photoelectrons corresponding to the "μ" in formulae (2) and (3)). The "σ_{1phe}" is the sigma of the Gaussian fit function for 1 photoelectron representing the "σ_1" in formula (3). And the "σ_{pedestal}" is the sigma of the Gaussian fit function for the pedestal indicating "σ_0" in formula (2).

Relying on these fit results, we can figure out how many photoelectrons correspond to an analog signal. For instance, if we have measured a signal similar to the one shown in Fig. 3, firstly we can calculate the number of photoelectrons – *N_phe* according to formula (1), then basing on the fit results of Fig. 4a, we can figure out the number of real photoelectrons by substituting X_{shift} = "1.06" and X_{scale} = "0.8781" into the following formula:

$$Real\ photoelectrons = (N\_phe - X_{shift}) \cdot X_{scale} \tag{5}$$

[1] Comparing to the QUARTIC (QUARtz TIming Cherenkov) which utilizes fused silica (artificial quartz) bars as radiators, the biggest advantage of the GASTOF is its much better intrinsic time resolution ($\sigma = 1.5$ ps) according to our simulation [1]. While as a gas detector, it has a typical weakness of low density. As a result, the number of Cherenkov photons produced by the GASTOF detector is much less than the QUARTIC one.

Although the QUARTIC has a worse intrinsic time resolution, it can be compensated by performing multiple measurements [1]. The latest paper [11] on the QUARTIC has shown that it can reach 10–20 ps time resolution (σ) depending on variant detector combinations with 120 GeV proton beam test data.

Actually, if the GASTOF is put in front of the QUARTIC along the direction of incident beam, there will be only very limited effects to the timing performance of the QUARTIC downstream due to very limited secondary and scattered particles produced by the GASTOF upstream thanks to its very few materials (including ~ 16 cm C_4F_{10} gas in ~ 1.1 atm, ~ 1.2 mm steel walls, and 3 mm mirror. Refer to Fig. 1a). Therefore these two kinds of detectors are complementary and it is possible to use them together.

[2] As a Cherenkov radiator, C_4F_{10} has been utilized in the RICH1 detector of the LHCb experiment.

[3] We got two tubes for each type of the MCP-PMTs. So the rise time etc have two values in each type.

[4] In experiments with the laser, the illuminated area of the MCP-PMT detector was observed by eyes to be ~ 8 mm in diameter; in the beam test, the radius of light spot is ~ 5 mm according to simulation.

[5] There is no amplifier between the MCP-MPTs and the oscilloscope, refer to Fig. 2.

[6] Plotted by ROOT [7].

[7] According to the data sheet of the MCP-PMT.

[8] To know the number of photoelectrons for an analog signal is not the only motivation of introducing the charge fit, a more important one is to do timing analysis – since we need to know the number of photoelectrons precisely in that case. Refer to Section 4.4, especially Eqs. (7)–(9).

[9] Eq. (2) was derived to fit the pedestal of the charge histogram. Eq. (3) was used to fit the non-pedestal part of the charge histogram. The whole fit function shown in Eq. (4) is to sum up these Poisson convoluted Gaussian functions then make a scaling on the events (y_{scale}).

[10] The "μ" is the average value of a Poisson function. The "X_{shift}", "X_{scale}" and "Y_{scale}" are a shift of the *X*-axis (charge), a scale of the *X*-axis (charge) and *Y*-axis (events) for a charge histogram separately. In Eq. (2), the "0" and "σ_0" are the mean value and sigma of the $Gauss(\hat{x}, 0, \sigma_0)$ where "$\hat{x}$" is $(x - x_{shift}) \cdot x_{scale}$. In Eq. (3), the "1" and "σ_1" are the mean and sigma of the $Gauss(\hat{x}, 1, \sigma_1)$, respectively; the "$n$" and "$\sqrt{n}\sigma_1$" is the mean and sigma of the $Gauss(\hat{x}, n, \sqrt{n}\sigma_1)$ separately. And for the laser test charge fit, we set $N = 20$.

[11] Because the *N_phe* was calculated from formula (1), so we name the unit of *X*-axis as 1 "calculated" photoelectron.

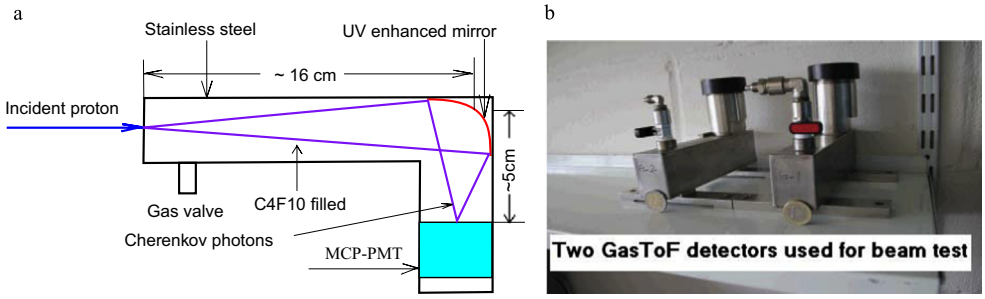

Fig. 1. Sketch of the GASTOF and two real ones. (a) Sketch of the GasTOF. (b) Two real GASTOFs.

Table 1
Comparison of two kinds of MCP-PMTs used in the laser test.

Items	Hamamatsu R3809U-50	Photek 210
Rise time (ps)	166 and 173	72 and 86
FWHM of TTS (ps)	25	No information
Spectral response range (nm)	160–850	214–800
Spectral peek wavelength (nm)	430	450
Resistance (MΩ)	200	420 and 132
Photocathode material	Multialkali	S20
Window material	Synthetic silica	Fused silica

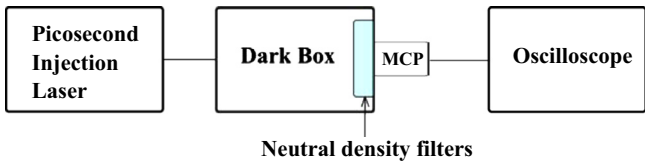

Fig. 2. Sketch of MCP-PMTs' laser test setup.

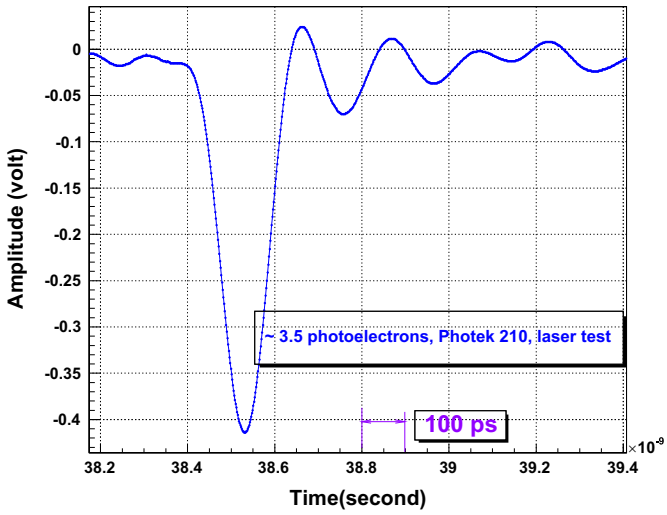

Fig. 3. A typical signal measured by a Photek 210 tube in the laser test.

3.3. Discussion on charge fit for the laser test

Comparing Fig. 4a and b, we can conclude the following[12]: (1) The Photek 210 tube has a better energy resolution than Hamamatsu R3809U-50. There exists distinct one and two photoelectrons' peaks in Fig. 4a but we cannot see any obvious one in Fig. 4b. Hamamatsu explained as "This is due to the saturation occurring in the MCP channel by the space charge effect" [4]. (2) The Photek tube has a better noise[13] performance than Hamamatsu one. The fit curve of Photek figure reaches the bottom of the pedestal's left side; while the Hamamatsu one cannot which means Hamamatsu tube's noise is non-Gaussian. Similar pedestal fit was observed on Hamamatsu tube by analyzing test beam data where the photons are Cherenkov light, refer to Fig. 9. In fact, we have checked from Refs. [4,8], but failed to see any pedestal included charge measurement histograms – the pedestals were all cut. So, we do not know whether the abnormal fit for the pedestals in Figs. 4b and 9 resulted from our measuring problem (s) or the Hamamatsu R3809U-50 tubes' intrinsic problem(s) or other unknown reason(s) due to the lack of comparison.

4. GASTOF beam test

4.1. The beam test setup

At the CERN SPS site, equipped with Hamamatsu R3809U-50 tubes, two GASTOF detectors were studied in the beam test.[14] The setup of our beam test is shown in Fig. 5. Two GASTOF detectors are upstream of the beam followed by two QUARTIC detectors.

The incident 120 GeV beam was composed of predominantly pions, and protons. The trigger was "$Trig_{logic\ plus}$=*Trig*_1 & *Trig*_2 & (! *Veto*)". "*Trig*_1" and "*Trig*_2" were plastic scintillators with a side length of ~3 cm which were read out by a Philips XP2020 PMT, "(!*Veto*)" was a $\phi \sim 30$ cm circle plastic scintillator with a $\phi \sim 2$ cm hole in the center which was also read out by a XP2020 PMT. This $Trig_{logic\ plus}$ is connected to an oscilloscope as a trig signal. Therefore, only the events which triggered *Trig*_1 and *Trig*_2 while did not trigger *veto* could be recorded in an oscilloscope.

The reason for designing this kind of trig is in order for both GASTOF detectors to produce equal numbers of photoelectrons. According to our simulation, the number of produced photoelectrons is proportional to the length of proton's trajectory inside a GASTOF [9]. To obtain the same number of photoelectrons in both detectors, beams must pass through the same length in two GASTOFs – that is to say it is better for beams to pass through both detectors' central lines. Therefore this kind of trigger logic setup was required. Since there were two QUARTIC detectors downstream of the GASTOF detectors, the scattered and secondary particles caused the veto scintillator being triggered very frequently. As a result, only a limited number of good events were recorded.

[12] Note that these two conclusions are not general statements on the comparison of two kinds of the MCP-PMTs. It is solely the results shown in our data.

[13] The "noise" in our data analysis corresponds to the signal of zero photoelectron. And this kind of signal is equivalent to the noise of a GASTOF in terms of the amplitude of charge. So, we adopted the notation of "noise" here.

[14] Only two Hamamatsu R3809U-50 tubes were tested with beam, the Photek 210 MCP-PMTs were not studied in the beam test. So from this section to the end of this paper, Both the "MCP_A" and "MCP_B" indicate the Hamamatsu R3809U-50 MCP-PMTs.

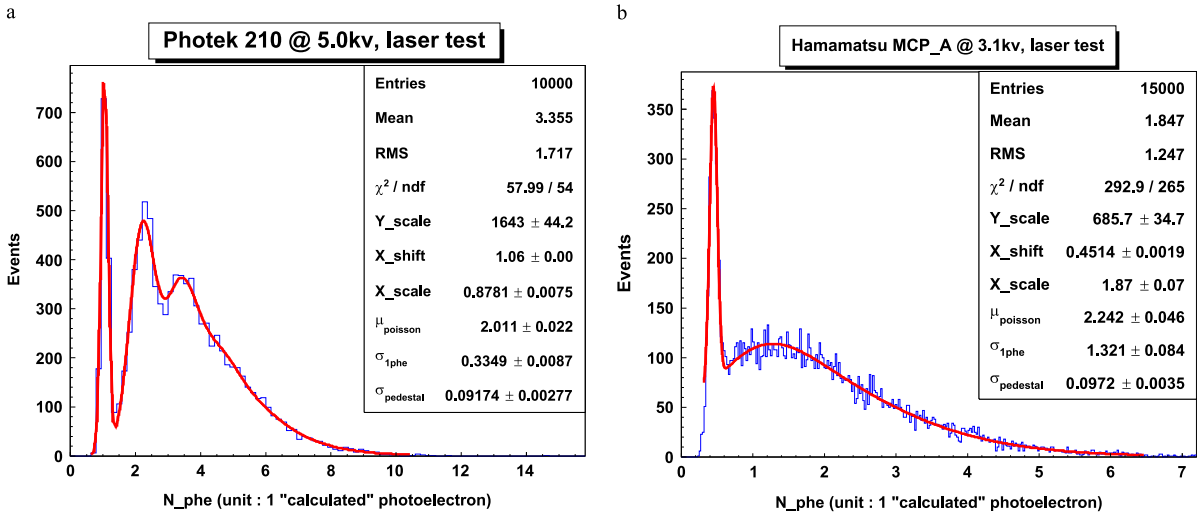

Fig. 4. Charge fit for Hamamatsu and Photek tubes in the laser test. (a) Photek 210. (b) Hamamatsu R3809U-50.

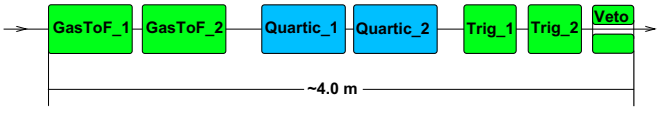

Fig. 5. Sketch of the beam test at CERN.

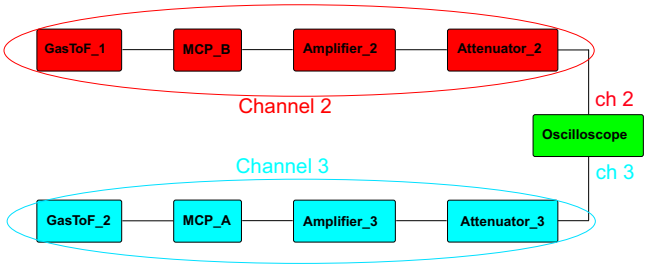

Fig. 6. Setup of the beam test at CERN.

Our detectors' setup in the beam test is shown in Fig. 6. There were two parallel channels, we name the upper one as channel 2 and the lower one channel 3.[15] The GASTOFs in two channels were identical and filled with the same pressure of C_4F_{10}. The high voltage for the MCP_B in channel 2 was set as 3.1 kV and the MCP_A in channel 3 was 3.25 kV.[16] The amplifiers provided by the Mini-circuits company are "ZX60-6013E +" which cover a bandwidth of 20 MHz–6 GHz with low noise. The attenuators are passive ones with a bandwidth up to 18 GHz. The oscilloscope has a wide bandwidth of 16 GHz and a sampling rate of 40 GSa/S when only two channels are taking data.[17] Fig. 7 shows a typical signal obtained from the beam test.[18]

Fig. 8 shows five analog signals measured by a GASTOF and the FFT (Fast Fourier Transform) analysis to these signals with Matlab [10]. From the FFT analysis result, we know that our signals have a frequency range roughly of 80 MHz–3 GHz. And this frequency range is inside the bandwidths of our DAQ chain: "amplifier+ attenuator + oscilloscope".

4.2. Charge fit of test beam data

Using the same fit function explained in Section 3.2, we performed a charge fit for beam test signals, as shown in Fig. 9. The "$\mu_{poisson}$" in the statistics box shows that the average number of photoelectrons was ~2.0 phe. The data obtained by the second parallel detector in channel 3 fitted almost the same number of photoelectrons.

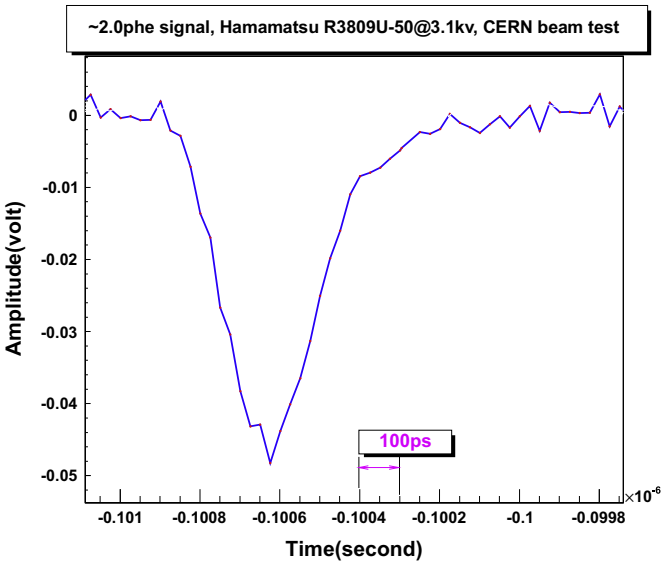

Fig. 7. A typical analog signal measured by Hamamatsu R3809U-50 from the beam test at CERN.

4.3. Timing analysis with method one

For the timing analysis of the test beam data, we developed two methods. The first method was to get the time resolution of a two GASTOF detectors system by subtracting the two detectors' timing directly, we call this "method one".

To get a signal's timing, a CFD (Constant Fraction Discriminator) algorithm was applied. The principle of the CFD algorithm is

[15] We named as channels 2 and 3 because these two chains were connected to channels 2 and 3 of the oscilloscope separately.

[16] For the two tubes we used in the beam test, according to the data sheet [4], the maximum supply voltage is −3.4 kV; and the recommended voltage range for one tube is −2.9 kV to −3.1 kV and another is −3.05 kV to −3.25 kV. Therefore, we set −3.1 kV and −3.25 kV to the tubes separately. For simplicity, we called them as "3.1 kV" and "3.25 kV".

[17] If all 4 channels are taking data at the same time, each channel is 20 GSa/S.

[18] Plotted by ROOT.

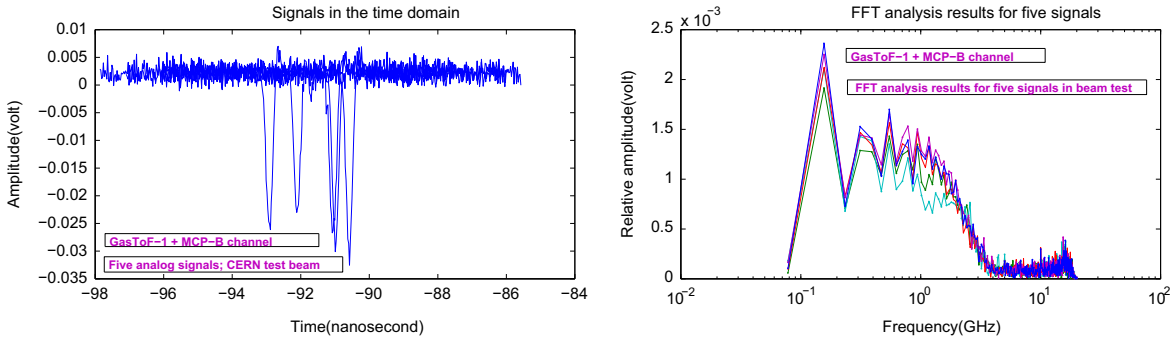

Fig. 8. Five analog signals obtained from the beam test at CERN and their FFT analysis with Matlab.

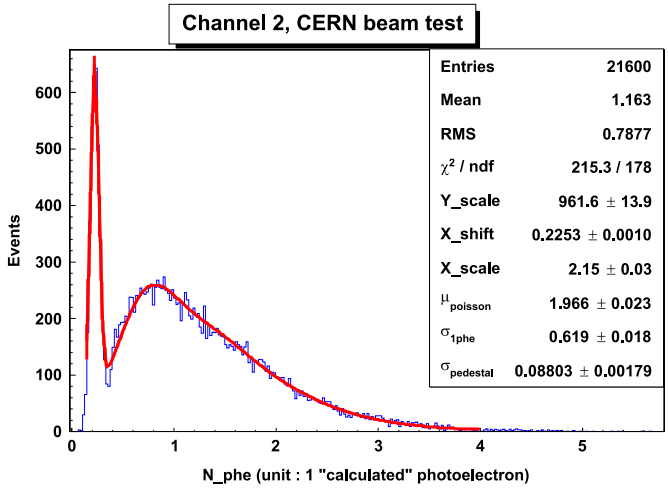

Fig. 9. A charge fit for the data obtained from the beam test at CERN.

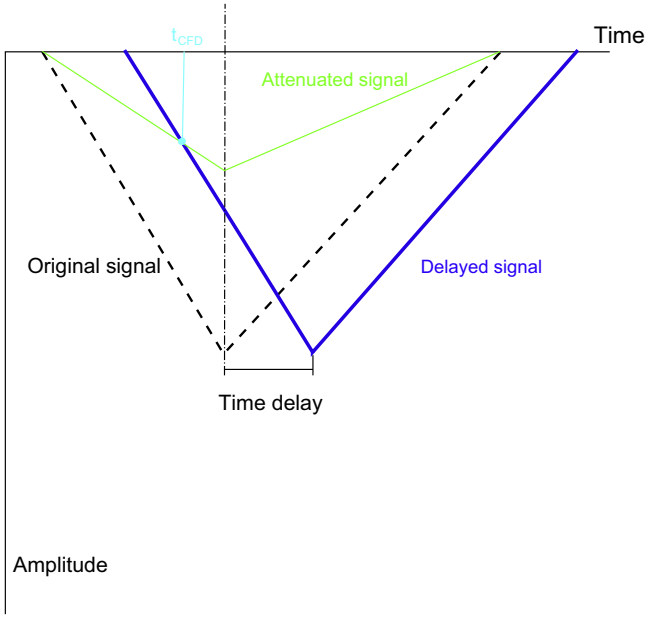

Fig. 10. The CFD algorithm.

shown in Fig. 10. The original signal is split into two channels, the delayed and the attenuated channel. The time crossing of these two channels is the CFD time: t_{CFD}.

Obtaining the CFD time of each GASTOF, we then performed a subtraction, $t_{CFD\ 1} - t_{CFD\ 2}$, or $T2$–$T3$ in our notation. Next, we made a Gaussian fit to the subtracted histogram of $T2$–$T3$, where the fitted σ represented a time resolution. One of the results is shown in Fig. 11: the time resolution of $T2$–$T3$ was $\sigma = 14.1$ ps.

For this analysis, signals from channel 2 were required to have more than 2 photoelectrons while signals from channel 3 were required to have more than 1.5 photoelectrons.[19] These cut resulted in an average charge value of ~ 3.6 phe in channel 2 and ~ 3.2 phe in channel 3, as shown in Figs. 12 and 13.[20]

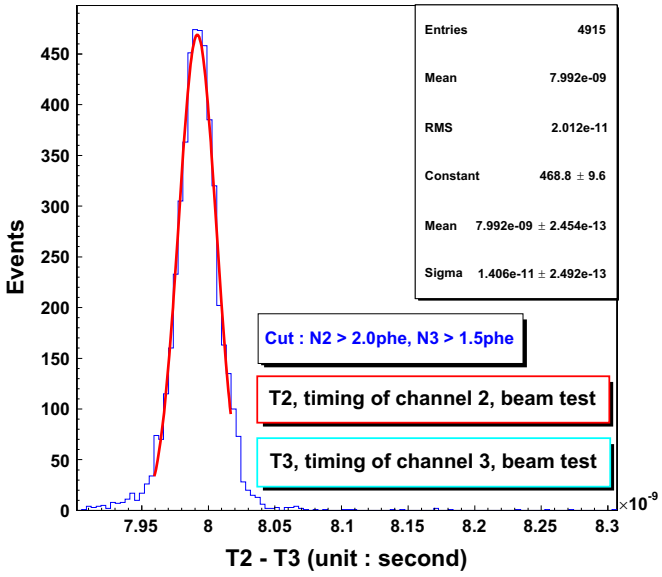

Fig. 11. A time resolution of $T2$–$T3$: $\sigma = 14.1$ ps which was analyzed by method one with CERN beam test data.

[19] These cut conditions were tuned from bigger phe cut to the final selected values of 1.5 phe and 2.0 phe. The criteria for selection of cutoff value were to have a consistent timing result by method two (formula (7)). The analysis is very sensitive to the cut of phe. As seen in Figs. 12 and 13 a very small change in the threshold will lead to a substantial change in the average number of photoelectrons due to its exponential dependence. And via formula (7), this change determines the consistency of timing by two methods (methods 1 and 2).

[20] From Fig. 12 to the end of this paper, the unit of X-axis of the charge histograms were all the "real" number of photoelectrons. Since we got a good charge fit as shown in Fig. 9, so we can rescale the X-axis of a charge histogram to the real number of photoelectrons by submitting corresponding fit results of "X_{shift}" and "X_{scale}" into formula (5). In fact, the method two of timing analysis relies on the real number of photoelectrons, if we do not know the real photoelectrons for N2 or N3, we cannot do analysis using formula (6) which played a key role for the timing analysis of method two.

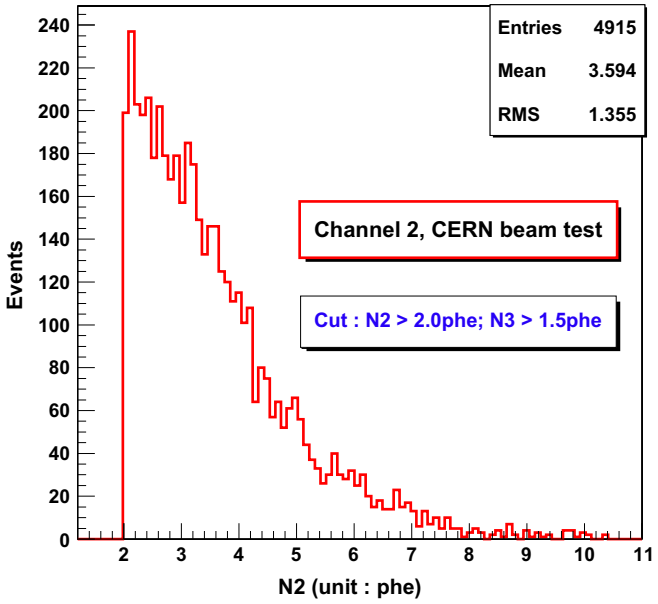

Fig. 12. With the selection of $N_2 > 2.0$ phe, $N_3 > 1.5$ phe, the average number of phe in channel 2≅3.6.

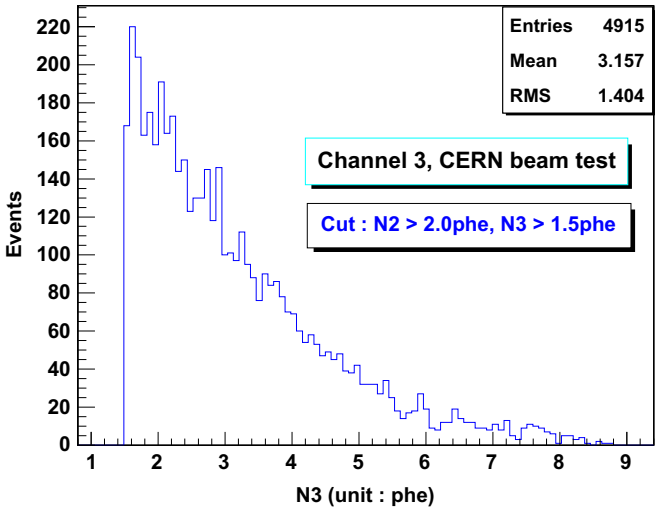

Fig. 13. With the selection of $N_2 > 2.0$ phe, $N_3 > 1.5$ phe, the average number of phe in channel 3≅3.2.

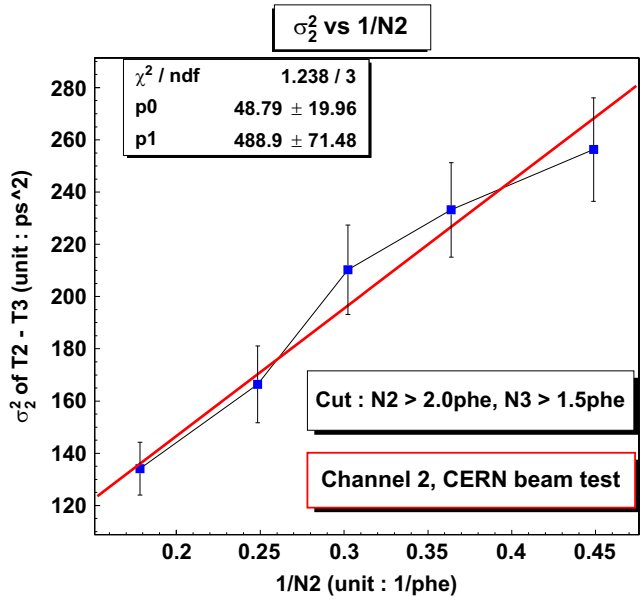

Fig. 14. Channel 2: σ_2^2 vs $1/N_2$.

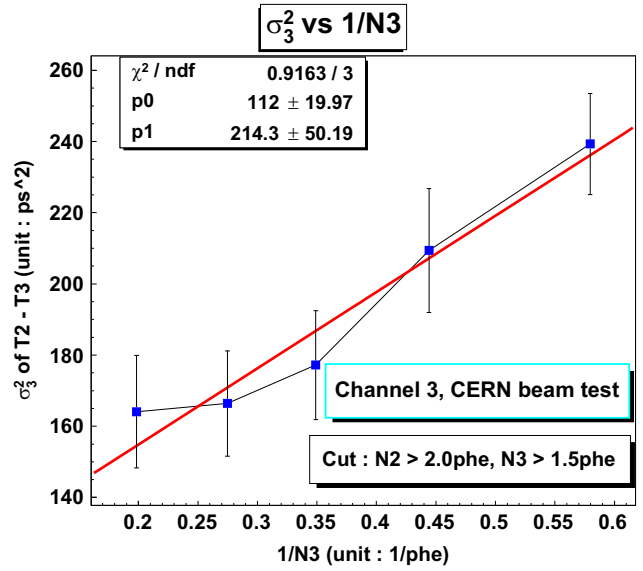

Fig. 15. Channel 3: σ_3^2 vs $1/N_3$.

4.4. Timing analysis with method two

Besides the method one, we developed another independent method to analyze timing which is named as "method two". The motivations for method two were (1) The HPS project's requirement on the time resolution of the GASTOF was based on an individual detector. So we need to determine each detector's contribution individually. While by method one, we only know the time resolution of a two GASTOFs' system. (2) It is necessary to do a cross-check to the result obtained by the method one.

In our beam test setup, the two GASTOF detectors were independent,[21] cf. Fig. 6. There therefore existed such a relation: $\sigma^2 = \sigma_{02}^2 + \sigma_{03}^2$, where σ is the sigma value of the Gaussian fit for the $T2$–$T3$ histogram (shown in Fig. 11) with contributions from the two GASTOF detectors individually: σ_{02} and σ_{03}. Moreover, because the produced photoelectrons followed a Poisson distribution, this relation can be expressed as

$$\sigma = \sqrt{\frac{\sigma_2^2}{N_2} + \frac{\sigma_3^2}{N_3}} \tag{6}$$

where "N_2" and "N_3" are the photoelectrons produced by the two detectors separately, "σ_2^2" and "σ_3^2" are the square of the time resolutions of 1 photoelectron for the corresponding detector.

The selection requirements applied in Section 4.3 resulted in an average number of photoelectrons of $N_2 = 3.6$ and $N_3 = 3.2$ (refer to Figs. 12 and 13). To calculate the right side of formula (6), we need to know σ_2^2 and σ_3^2. We got them by fitting "σ_i^2" vs "$1/N_i$" ($i = 2, 3$) to each channel. The linear-fit results were shown in Figs. 14 and 15. In every figure, "$p1$" is the value of σ_i^2 for one

[21] There was no common noise source for two channels for they were totally independent.

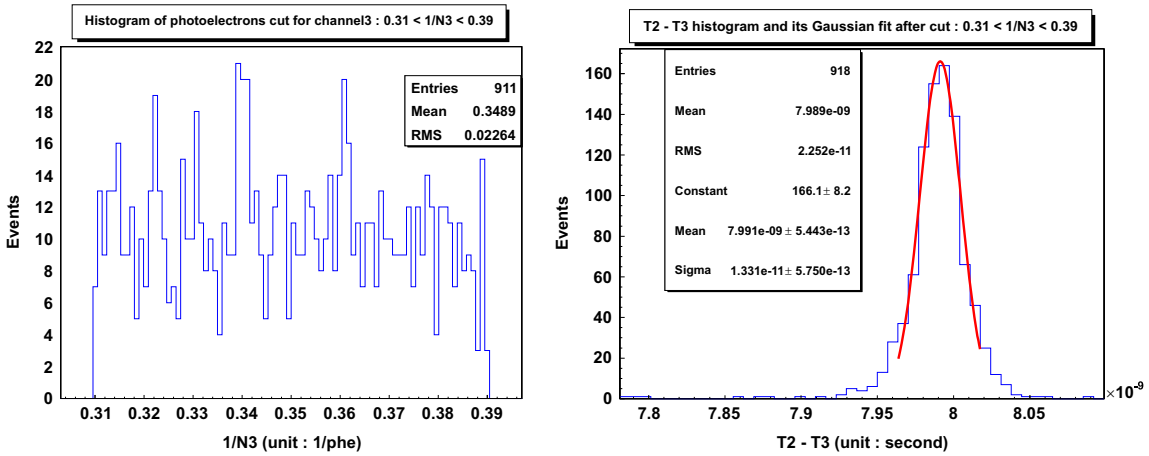

Fig. 16. Charge cut $0.31 < 1/N3 < 0.39$ and the corresponding $T2$–$T3$ histogram with a Gaussian fit.

photoelectron, and "$p0$" is the best time resolution of the referenced channel can reach.[22]

In Figs. 14 and 15, every figure contains 5 points. The X-axis of these points resulted from the mean values of the corresponding charge selections. For instance, in the left sub-figure of Fig. 16, the charge selection is "$0.31 < 1/N_3 < 0.39$", the mean value of $1/N_3$ under this selection is 0.3489. Applying the same charge selection, the $T2-T3$ histogram and its Gaussian fit is shown in the right sub-figure of Fig. 16. Squaring the "Sigma" value in the right sub-figure, we obtain $(13.31)^2 = 177.2$. The "0.3489" and "177.2" are the X and Y values of the third point in Fig. 15 (count from left to right). The X and Y values of other four points of Fig. 15 are shown in Table 2. Similarly, Fig. 14 has its values in Table 3.

By substituting parameters to the right side of formula (6): $\sigma_2^2 = p1 = 488.9 \pm 71.5$ (refer to Fig. 14), $\sigma_3^2 = p1 = 214.3 \pm 50.2$ (refer to Fig. 15), $N_2 = 3.6$ phe (Fig. 12) and $N_3 = 3.2$ phe (Fig. 13), we obtain

$$\sqrt{\frac{\sigma_2^2}{N_2}+\frac{\sigma_3^2}{N_3}} = \sqrt{\frac{488.9 \pm 71.5}{3.6}+\frac{214.3 \pm 50.2}{3.2}} = 14.2 \pm 0.89 \text{ ps} \quad (7)$$

This was consistent well with the result in Fig. 11: 14.1 ± 0.25 ps.

Moreover, from formula (7), we can determine the time resolution for channel 3:

$$\sigma_{ch3} = \sqrt{\frac{\sigma_3^2}{N_3}} = \sqrt{\frac{214.3 \pm 50.2}{3.2}} = 8.2 \pm 0.96 \text{ ps} \quad (8)$$

That is to say, for channel 3, under the cut condition of $N2 > 2.0$ phe, $N3 > 1.5$ phe, its time resolution reached ~ 8.2 ps.

Similarly, the time solution of channel 2 is

$$\sigma_{ch2} = \sqrt{\frac{\sigma_2^2}{N_2}} = \sqrt{\frac{488.9 \pm 71.5}{3.6}} = 11.7 \pm 0.85 \text{ ps} \quad (9)$$

[22] Take Fig. 14 as an example first, in case $1/N2 = 0$, $\sigma_2^2 = 48.8$ ps $\Rightarrow \sigma_2 = 7.0$ ps. If the N2 had infinity photoelectrons its contribution to a time jitter would be negligible, so only the N3 or channel 3 contributed to the σ_2^2. As a result, this $\sigma_2 = 7.0$ ps actually should be interpreted as $\sigma_3 = 7.0$ ps in the case of the selection shown in Fig. 14 and $1/N2 = 0$. Similarly, $\sigma_2 = \sqrt{112} = 10.6$ ps with the selection shown in Fig. 15 and if $1/N3 = 0$. So, from the comparison of $p0$, the $p0$ in channel 3 was better than channel 2. This was consistent with the comparison of $p1$ which represented σ_i^2 per one photoelectron: 214.3 of channel 3 was better than 488.9 of channel 2.

Table 2
The original data of Fig. 15.

Points (count from left to right)	X (1/phe)	$Y \pm \sigma_Y$ (ps^2)
First point	0.20	164.1 ± 15.8
Second point	0.27	166.4 ± 14.8
Third point	0.35	177.2 ± 15.3
Fourth point	0.44	209.4 ± 17.4
Fifth point	0.58	239.3 ± 14.2

Table 3
The original data of Fig. 14.

Points (count from left to right)	X (1/phe)	Y $\pm \sigma_Y$ (ps^2)
First point	0.18	134.1 ± 10.1
Second point	0.25	166.4 ± 14.7
Third point	0.30	210.3 ± 17.1
Fourth point	0.26	233.2 ± 18.1
Fifth point	0.45	256.3 ± 19.8

4.5. Discussion on timing analysis

From Figs. 14 and 15, the $p1$ values for the two channels were 488.9 and 214.3, which corresponded to 22.1 ps ($\sqrt{488.9}$) and 14.6 ps ($\sqrt{214.3}$) for one photoelectron. They were variant and both worse than the value of 25 ps (FWHM) = 10.6 ps (σ) for one photoelectron according to Table 1.

Three main factors affect the time resolution of GASTOF: (1) the spread in arrival time of the photons at the photocathode, (2) the time resolution of the MCP-PMT, which is dominated by the transit time spread (TTS) of electrons from emission at the photocathode to arrival at the anodes, and (3) the downstream electronics, including signal dispersion in cables [1]. Our simulation indicated GASTOF only introduced a time jitter of $\sigma \sim 1.5$ ps [9].[23] According to our measurement in the lab, the electronics contributed around $\sigma \sim 4.2$ ps in the case of average ~ 2 phe signals. So we thought that the time resolution of our system mainly depended on the TTS of MCP-PMTs. Probably the timing performance of our

[23] The main reasons response for such a small time jitter are (1) The Cherenkov angle is very small, around 3°; (2) the distance of photons' propagation is roughly 20 cm (in 1.1 atm C_4F_{10}); (3) the diameter of the input window of Hamamatsu tube is roughly 1 cm; (4) the detector's mechanical design was optimized; and (5) our simulation supported this result [1].

Hamamatsu tubes had degraded a little after a few years usage.[24] Besides, although the low frequency noises were constrained by the amplifier which has a bandwidth of 20 MHz–6 GHz, our FFT analysis of analog signals still shows some high frequency (for instance >6 GHz) noises caused by unknown sources, refer to Fig. 8. This part of noises would have a negative effect on the time resolution.

5. Conclusion and outlook

Based on the test beam data, we found that one single GASTOF can reach a time resolution of $\sigma \sim 8.2$ ps under the cut of $N2 > 2.0$ phe, $N3 > 1.5$ phe (on average, ~ 2 phe in both channels). Another one reached $\sigma \sim 11.7$ ps time resolution under the same selection.

From Figs. 14 and 15, we think that the more the photoelectrons produced, the better the time resolution would reach. So, the next generation of the GASTOF detectors will focus on increasing the number of photoelectrons. For instance, with side mirrors to improve the Cherenkov light collection, and using the MCP-PMTs with a MgF2 window to increase the UV sensitivity.[25] The expected signal for the same detector size is of 4–5 photoelectrons[26] on average (currently, it is $\approx$2.0 phe, refer to Fig. 9).

Additionally, some studies are necessary for deeper understanding on the GASTOF. (1) The detector efficiency. We never tested this critical parameter for our GASTOFs. In CERN test beam, it is too tight for us to schedule such a test. (2) The lifetime of the MCP-PMTs and the possible ways to improve it, like searching bigger gain amplifier then the HV of the MCP-PMTs, can be decreased therefore the lifetime of the MCP-PMTs is supposed to be extended, or replacing them with the SiPMs [11]. (3) Using the Photek 210 tubes as a photons' detector to read the GASTOF's signals out. It is pity we never studied "Photek 210+GASTOF" in the beam test though the results were supposed to be better than the current ones according to (a), a Photek tube has a typical rise time of ~ 80 ps while a Hamamatsu one is of ~ 160 ps; (b), our preliminary comparisons in lab by laser pulses shown that a Photek's timing performance is better than a Hamamatsu one.

[24] We bought them in 2008. And during the past years, we did not test them very frequently but had some usages including beam tests and cosmic ray tests.

[25] For instance, replacing the currently used R3809U-50 with the R3809U-58. MgF2 window will increase the number of photoelectrons by larger spectral range of acceptance as MgF2 transmission cut of at 115 nm, while present silica at 160 nm.

[26] with C_4F_{10}, the photon yield for $\beta \approx 1$ charged particle is ~ 30 [3].

Acknowledgments

We thank Dr. Nicolas Schul and Dr. Tomasz Pierzchala, our former colleagues in UCLouvain, who had been involved deeply in this project for years and contributed significantly in many aspects. Also, we thank our (former) colleagues in UCLouvain Dr. Pavel Demin and Dr. Jérôme de Favereau for their computer related support. And we thank Dr. Jonathan Hollar for his help on manuscript revision. In addition, we would like to thank Prof. Andrew Brandt from the University of Texas, Alington, USA who organized the beam test at SPS, CERN. We thank Dr. Hasko Stenzel from
the University of Geissen, Germany and Dr. Shengli Liu from the University of Alberta, Canada who contributed a lot to the beam test.

Also, we thank the anonymous reviewers who have presented their professional and insightful comments which improved the quality of this paper in many aspects comparing to the first version of our submission.

References

[1] M.G. Albrow, et al., Journal of Instrumentation (2009) JINST_001T_1208.
[2] K. Piotrzkowski et al., R&D of the detectors systems for Stage One of the High Precision Spectrometer Project (Internal Document).
[3] ⟨https://twiki.cern.ch/twiki/bin/view/LHCb/C4F10⟩.
[4] MCP-PMT R3809U-50 final test sheet, Hamamatsu Photonics K.K.
[5] Photek Test Summary, 23080605 and 23081104, Photek Limited.
[6] PiLas Test Report (A Dedicated Test Report Issued by Advanced Laser Diode Systems A.L.S. GmbH in Mar, 2007).
[7] ⟨http://root.cern.ch/drupal/⟩.
[8] Photomultiplier tubes, basics and applications, edition 3a, Hamamatsu, 51.
[9] Measurements of two-photon interactions at the LHC (Doctoral dissertation), Nicolas Schul, UCLouvain.
[10] ⟨http://www.mathworks.ch/products/matlab/⟩.
[11] A. Ronzhin, et al., Nuclear Instruments and Methods in Physics Research Section A 623 (2010) 931.